

HiSST: 4th International Conference on High-Speed Vehicle Science Technology

22 -26 September 2025, Tours, France



Numerical Investigation on the Optimization of a Detonation-Assisted Fuel Injection System for Scramjet Engines under Mach 8 Flight Conditions

M. Miyashita¹, A. Matsuo², E. Shima³, N. Itouyama⁴, A. Kawasaki⁵, K. Matsuoka⁶, J. Kasahara⁷

Abstract

A novel detonation-assisted fuel injection system was developed to achieve highly efficient supersonic combustion in scramjet engines. While previous studies employed an annular Rotating Detonation Combustor (RDC) arranged coaxially around the main fuel injector, this study introduced a simplified cylindrical RDC configuration to enhance practicality and structural feasibility. In this design, both the main fuel and detonation products were injected from the same bottom-mounted configuration into a Mach 2.4 supersonic flow, simulating flight conditions at Mach 8.0 and an altitude of 30 km. A stoichiometric premixed H₂-O₂ mixture was supplied to the cylindrical RDC, where continuous detonation propagation was sustained even when connected to the main combustor. As a result, the detonation products were discharged, effectively entraining the main fuel and promoting rapid mixing and combustion. The hydrogen jet formed a characteristic helical distribution as it interacted with the rotating detonation wave. Despite the geometric simplification, the cylindrical RDC achieved a fuel consumption rate comparable to that of the annular RDC, while reducing the required combustor length by 23.3% compared to a baseline model without detonation assistance. These results demonstrate that, even without an inner annular structure, the cylindrical RDC can maintain high combustion efficiency and offer a more compact and practical configuration for future scramiet applications.

Keywords: detonation, scramjet engine, cylindrical Rotating Detonation Engine, computational fluid dynamics, supersonic combustion

Nomenclature

p - pressure

T - temperature

M - Mach number

 ${\it J}$ - dynamic pressure ratio relative to the main flow

d_{fuel} - diameter of the main fuel injection port

 d_{RDC} - diameter of the RDC

m - mass flow rate

q - heat release rate

A - cross-sectional area of the combustor

 η_m = fuel consumption rate

Subscripts

s - static condition

infinity - condition of the supersonic airflow jet - condition of the main fuel for combustion in the supersonic airflow

infinity - condition of the supersonic airflow

Page | 1

¹ Keio University, 3-14-1 Hiyoshi Kouhoku-ku Yokohama Kanagawa Japan, moenomiyashit@keio.jp

² Keio University, 3-14-1 Hiyoshi Kouhoku-ku Yokohama Kanagawa Japan, matsuo@mech.keio.ac.jp

³ Keio University, 3-14-1 Hiyoshi Kouhoku-ku Yokohama Kanagawa Japan, shima.eiii@iaxa.ip

⁴ Nagoya University, Furo-cho Chikusa-ku Nagoya Aichi Japan, itouyama@imass.nagoya-u.ac.jp

⁵ Shizuoka University, 3-5-1 Jyohoku Naka-ku Hamamatsu Shizuoka Japan, kawasaki akira@shizuoka.ac.jp

⁶ Nagoya University, Furo-cho Chikusa-ku Nagoya Aichi Japan, matsuoka@nuae.nagoya-u.ac.jp

Nagoya University, Furo-cho Chikusa-ku Nagoya Aichi Japan, kasahara@nuae.nagoya-u.ac.jp HiSST-2025-338



HiSST: 4th International Conference on High-Speed Vehicle Science Technology 22 -26 September 2025, Tours, France



1. Introduction

The Scramjet engines have long attracted attention as a promising air-breathing propulsion system for hypersonic flight. They can achieve more than ten times the specific impulse of conventional rocket engines and are increasingly regarded as a key technology for reusable, low-cost space transportation systems [1]. Recent advances have demonstrated the feasibility of scramjet propulsion. In Japan, JAXA successfully conducted in-flight supersonic combustion at Mach 5.8 using the S-520-RD1 sounding rocket in 2022 [2]. In addition, flight experiments conducted in various countries, including NASA's X-43A [3] and X-51A [4] programs and the internationally coordinated HyShot [5] and HiFiRE programs [6], have contributed significantly to the understanding of scramjet operability and combustion stability under hypersonic flight conditions.

Despite these advances, the practical implementation of scramjet propulsion remains limited. Due to the supersonic inflow of atmospheric oxidizer, the residence time of the fluid in the combustor is limited to only a few milliseconds [7]. This presents a major challenge to achieving stable and efficient combustion. To overcome the associated difficulties, various fuel injection strategies have been proposed in recent years. Macleod [8] recently reviewed the effects of injector design parameters, including geometry, placement, and injection conditions, on mixing and combustion characteristics. For example, strut and coaxial injectors have demonstrated superior mixing and fuel penetration, particularly under high-Mach-number conditions, while additional strategies such as upstream pre-injection and staged injection have been employed to enhance flame-holding and fuel consumption efficiency by inducing thermal stratification and spatially controlling reactivity [9-12]. However, although various strategies have been explored, a sufficiently effective solution has yet to be established, and continued research is required to advance the practical application of scramjet propulsion systems.

To address these limitations, this study focuses on a novel approach that utilizes detonation combustion as an energy source to assist combustion in scramjet engines, which proposed by our previous study [13]. Detonation is a self-sustained combustion wave driven by shock-induced compression. It is considered a promising technology for next-generation rocket engines, offering a significantly shorter combustion completion length and achieves over 10% improvement in thermal efficiency compared to conventional cycles such as the Brayton cycle [14]. Among various detonation-based applications, the Rotating Detonation Combustor (RDC) has received particular attention. The RDC produces continuous detonation propagation at frequencies of 1–100 kHz within an annular or cylindrical combustor, generating high-enthalpy and unsteady detonation products in a compact configuration [15]. Such characteristics suggest that detonation product is considered an energy source for promoting combustion thermally and chemically, and for enhancing mixing through unsteadiness-induced hydrodynamic effects in supersonic flows.

Given this background, the present study builds upon our previous work, which proposed a detonation-assisted fuel injection system using high-enthalpy burned gas to enhance supersonic combustion. Although an annular RDC was employed as a simplified configuration in the earlier study, it poses practical challenges such as excessive thermal loading on the inner wall. To overcome these limitations, the objective of the present study is to adopt a more practical cylindrical RDC geometry and to conduct three-dimensional numerical simulations to clarify the internal flowfield and the resulting combustion in the mainstream, thereby supporting the optimization of combustor geometry for future detonation-assisted scramjet systems.

HiSST-2025-338 M. Miyashita , A. Matsuo , E. Shima , N. Itouyama , A. Kawasaki , K. Matsuoka , J. Kasahara

2. Target Geometry of a Detonation-Assisted Fuel Injection System Using a Cylindrical RDC

This section first introduces the baseline injection model used as a reference in this study. As illustrated in Fig. 1(a), the baseline configuration simulates a conventional scramjet combustor, in which the main fuel is vertically injected into the supersonic crossflow through a single orifice. This configuration represents one of the most fundamental fuel injection schemes for scramjet engines and is consistent with the experimental and numerical setups previously investigated by Gamba et al. [16].

In the following, Fig. 1(b) presents the "annular RDC model" employing a annular RDC, which was proposed in our previous study as a simplified detonation-assisted injection configuration. In this model, an annular RDC is arranged around the central fuel injector to continuously generate highenthalpy detonation products containing unsteady pressure waves and reactive radicals. These burned gases are co-injected with the main fuel through a concentric dual-orifice. The configuration is intended to enhance combustion efficiency by leveraging two primary mechanisms: (1) thermal and chemical assistance through the penetration of hot, radical-rich detonation products, and (2) enhancement of large-scale vortex formation induced by the introduction of unsteady pressure disturbances into the mainstream.

To further address the thermal and structural challenges associated with the inner wall of the annular geometry and to improve practicality, the present study adopts a more compact cylindrical RDC configuration. Figure 2 presents a schematic of the proposed cylindrical RDC model. In this geometry, the main fuel injection port—identical to that used in the baseline model—is located at the center of the bottom surface of the single-cylinder combustor. The main fuel is injected into the RDC and mixes with the continuously generated detonation products before being exhausted. This configuration is expected to serve as a more feasible alternative for integration into scramjet engines while maintaining the benefits of thermal and chemical assistance.

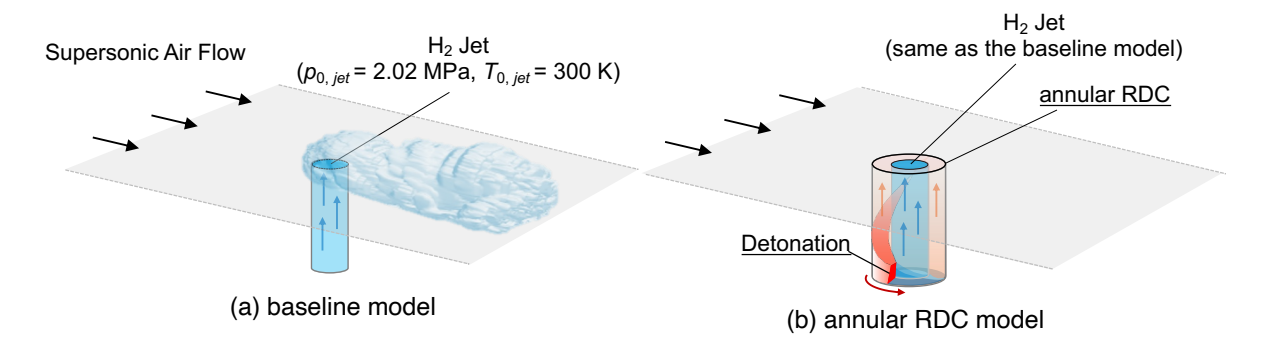


Fig 1. Schematic images of (a) the baseline model based on Gamba et al. [16], used as a reference for comparison, and (b) annular RDC model which proposed by Miyashita et al. [13] as a detonation-assisted fuel injection system.

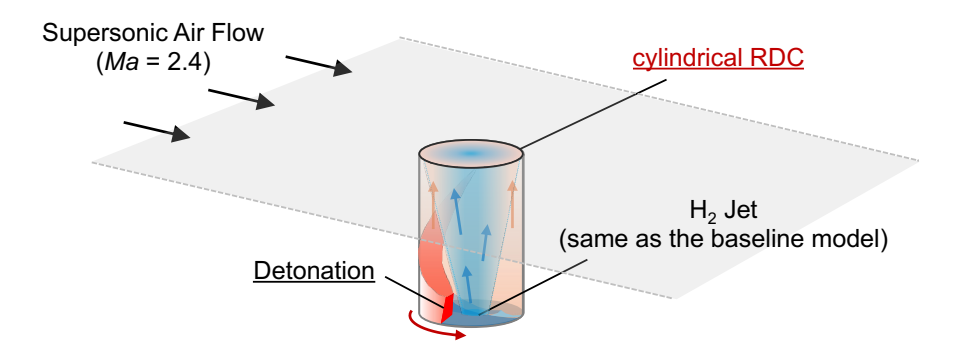


Fig 2. Schematic image of the cylindrical RDC model, which features a more practical geometry than the conventional annular RDC model.

HiSST-2025-338 Page |3 Numerical Investigation on the Optimization of a Detonation-Assisted Fuel Injection System

3. Numerical Methods

In this study, the three-dimensional compressible Reynolds-Averaged Navier-Stokes (RANS) equations were adopted in the simulation of the supersonic mainstream flow field. These governing equations represent the conservation of mass, momentum, energy, and species mass fractions for nine chemical species: H₂, O₂, H, O, OH, H₂O, HO₂, H₂O₂, and N₂. The equation of state was modeled under the assumption of a thermally perfect gas. For the RDC region, the three-dimensional Euler equations were used, as our preliminary calculations confirmed that viscous effects were negligible in this area. In contrast, the remainder of the computational domain—that is, the entire region excluding the RDC was computed with full inclusion of viscous terms. The convective fluxes were discretized using the third-order AUSM-DV scheme [17], with MUSCL reconstruction [18] applied to improve spatial accuracy near discontinuities. Diffusive terms were discretized using a second-order central difference scheme. Time integration was performed using a three-stage, third-order total variation diminishing (TVD) Runge-Kutta method [19]. Note that, the time step was set on the order of 1.0×10^{-9} s, which is sufficiently smaller than the characteristic time scale of detonation wave rotation (on the order of 1.0×10⁻⁵ s). As confirmed by our preliminary calculations, this temporal resolution allows the unsteady features induced by detonation propagation to be accurately captured, even when using the RANS formulation. Chemical reactions were modeled using the detailed kinetic mechanism developed by Hong et al. [20], which has already been widely validated in detonation simulations. Thermodynamic properties were evaluated using NASA polynomial fits [21], while viscosity (µ) and thermal conductivity (κ) were computed based on the method of Gordon [22]. The Wilcox $k-\omega$ turbulence model [23] was employed for closure of the RANS equations.

4. Calculation Targets

This section describes the computational setup employed in the present study. As summarized in Table 1, three configurations are considered. The central focus is placed on the cylindrical RDC model, which is newly proposed to investigate a more practical combustor geometry suitable for integration into scramjet engines. For comparative purposes, two reference cases are also analyzed: the baseline model and the annular RDC model. Both models, introduced in Section 2, follow the configurations adopted from Ref. [13].

4.1. Supersonic Mainstream Flow Conditions

The computational grid and boundary conditions for the supersonic mainstream region are shown in Fig. 3. Based directly on the experimental and assumed flight conditions reported by Gamba et al. [16], the present study analyzed the flow field of a scramjet engine at a flight altitude of 30 km and a flight Mach number of 8.0. The airflow within the combustor was assumed to be dry air, with a Mach number M_{∞} of 2.4, a static pressure $p_{s,\infty}$ of 40 kPa, and a static temperature $T_{s,\infty}$ of 1580 K. As shown in Fig. 1(a), the baseline model employed for comparison followed the vertical and choked fuel injection configuration used in the previous experimental study [16]. Hydrogen was used as the main fuel, with a total pressure $p_{0,\rm jet}$ of 2.02 MPa and a total temperature $T_{0,\rm jet}$ of 300 K. The dynamic pressure ratio J relative to the supersonic mainstream was set to 5.0, and the mass flow rate of the hydrogen jet $\dot{m}_{\rm H_2,\rm jet}$ was 3.92 g/s, which corresponds to a global equivalence ratio of approximately 0.12 for the entire domain. The diameter of the vertical injection port was 2 mm, which was used as the reference length $d_{\rm fuel}$. The computational domain extended 180 $d_{\rm fuel}$ in the streamwise (x) direction, 40 $d_{\rm fuel}$ in the vertical (y) direction, and 45 $d_{\rm fuel}$ in the spanwise (z) direction. The injection port was positioned at $x=30d_{\rm fuel}$ and $z=22.5d_{\rm fuel}$. The boundary conditions and the grid spacing were used the same as our previous study[16].

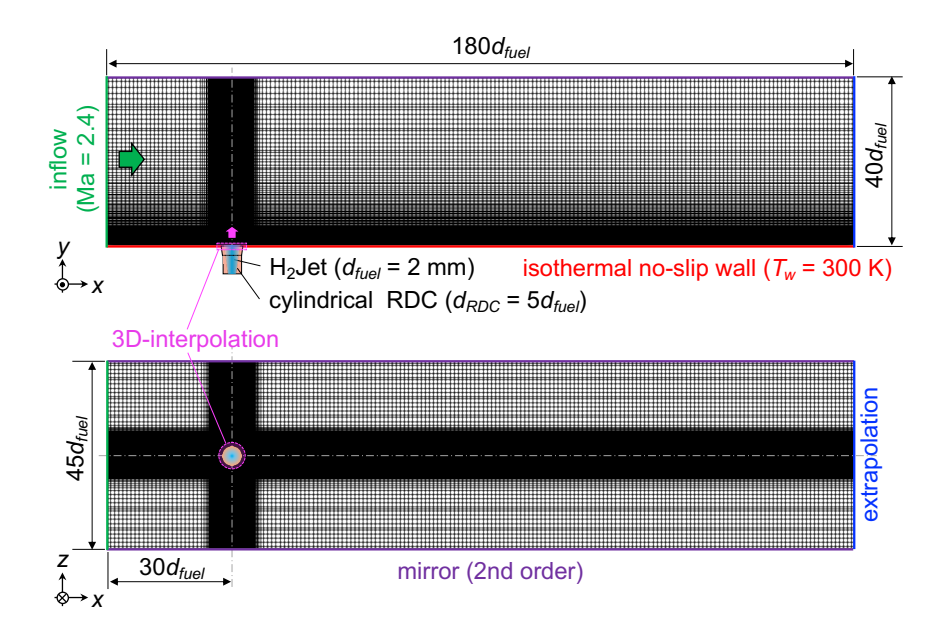


Fig 3. Computational grid and boundary conditions used for the analysis of the mainflow region. The representative length was set to $d_{\text{fuel}}=2.0 \text{ mm}$ [13].

4.2. Cylindrical RDC conditions

As shown in Fig. 4, the cylindrical RDC section, with a diameter d_{RDC} of $5d_{fuel}$, consists of a straight combustor with a constant cross-sectional area, followed by a divergent nozzle. A polar mesh was employed for the RDC, containing 1005 grid points in the circumferential direction, along which the detonation wave propagates. The grid width in this direction was approximately 31 µm, corresponding to a resolution of about six points per induction length in detonation combustion. Furthermore, an orthogonal mesh was adopted to prevent the occurrence of singularities. A total of 24 injector pairs were installed at the base of the combustor to supply the fuel and oxidizer required for detonation combustion. These propellants were injected through opposing injectors inclined at 45° relative to the axial direction. The main fuel injector was also installed at the center of the bottom surface, as shown in Fig. 4. The supply conditions for the fuel and oxidizer used in this study are summarized in Table 1. Hydrogen—identical to that used as the main fuel in the combustor—was employed as the fuel, and oxygen was used as the oxidizer. To reduce computational cost, viscous effects within the RDC were neglected, and the flow field was computed using the Euler equations. The propellant mixture supplied to the RDC was a stoichiometric premixed gas. The mass flow rate of hydrogen supplied to the RDC, $\dot{m}_{\rm H_2,RDC}$ was set to 35% of that of the main fuel. Note that the conditions for the baseline model and the annular RDC model were directly adopted from our previous study [13].

The boundary conditions for the RDC were defined as follows. The walls of the combustor and nozzle were treated as adiabatic slip walls. At the injector surface, the inflow condition dynamically switched between choked inflow, subsonic inflow, and no inflow, depending on the pressure just above the injector surface. The outlet of the divergent nozzle was connected to the lower wall of the supersonic mainstream region, representing a scramjet combustor. At this junction, conservative variables were interpolated in three dimensions at every time step to enable coupled simulations.

HiSST-2025-338 Page |5

Table 1 Design mass flow rates, total pressure and temperature of the supplied propellants, and dynamic pressure ratios relative to the mainstream for each case.

	<i>m</i> _{H2,jet} [g/s]	p _{0,jet} [MPa]	7 _{0,jet} [K]	<i>m</i> _{H₂,RDC} [g/s]	<i>m</i> _{O₂,RDC} [g/s]	p _{0,RDC} [MPa]	7 _{0,RDC} [K]	<i>m</i> _{total} [g/s]	dynamic pressure ratio J
baseline model (H ₂ jet only)	3.92	2.02	300	-	-	-	-	3.92	5.0
annular RDC model	3.92	2.02	300	1.53	12.12	1.5	298	3.92 (H ₂ jet) 13.65(RDC)	5.0 (H ₂ jet) 1.0 (RDC)
cylindrical RDC model	3.92	2.02	300	1.53	12.12	1.5	298	3.92 (H ₂ jet) 13.65 (RDC)	1.0

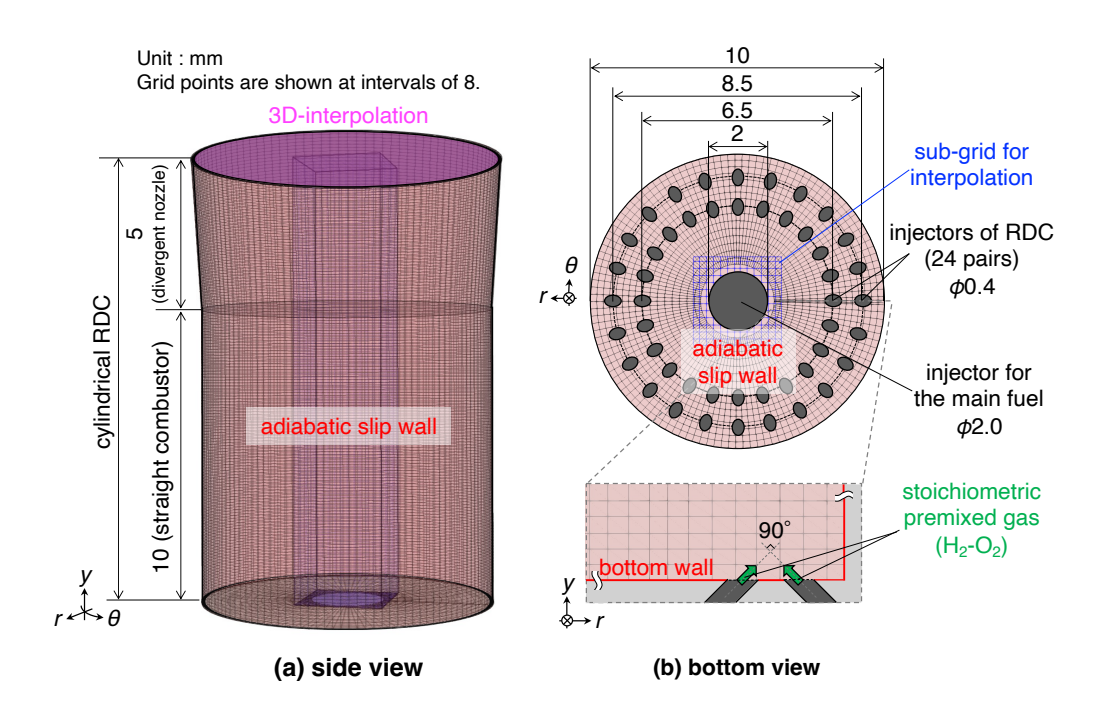


Fig 4. Computational grid and boundary conditions of the cylindrical RDC section connected to the mainstream region: (a) side view and (b) bottom view including the injection configuration.

5. Results and discussion

5.1. Flow and Combustion Characteristics within the cylindrical RDC

Figure 5 presents the time evolution of the internal flowfields for the two configurations considered: (a) the annular RDC model and (b) the cylindrical RDC model. In both cases, iso-surfaces of pressure were visualized to capture the propagation of the detonation wave. In addition, for the cylindrical RDC case, iso-surfaces of hydrogen mole fraction—colored in blue—were included to illustrate the main fuel transport. In the annular RDC model, stable propagation of the detonation wave along the outer wall was observed. The propagation was accompanied by the formation of oblique shock waves extending toward the downstream end of the combustor, i.e., the interface with the supersonic mainstream region. In the cylindrical RDC case, the pressure levels and propagation speed of the detonation wave were comparable to those observed in the annular configuration. However, the main fuel injector was placed at the center of the bottom wall, resulting in a distinct fuel transport behavior. As indicated by the blue iso-surfaces, hydrogen was discharged from the injector and flowed toward the combustor exit. This

HiSST-2025-338 Page |6 M. Miyashita , A. Matsuo , E. Shima , N. Itouyama , A. Kawasaki , K. Matsuoka , J. Kasahara Copyright © 2025 by author(s) fuel jet was disturbed by the detonation propagation and formed a complex distribution characterized by a spiraling structure, as it appeared to follow and interact with the rotating detonation front.

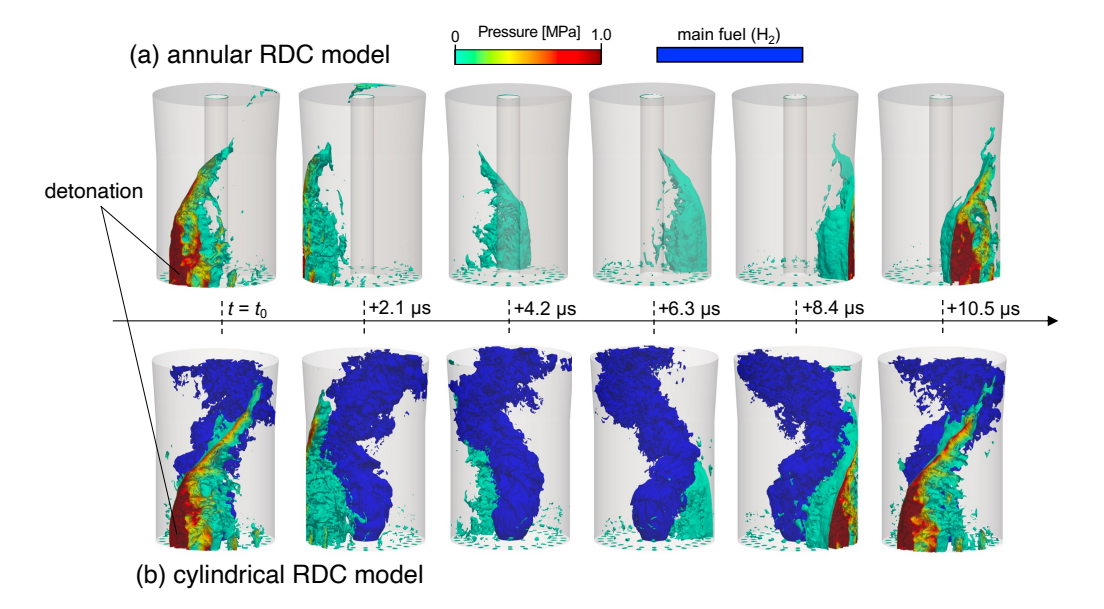


Fig 5. Time-resolved pressure and H₂ distributions in the RDC section analysed in conjunction with the mainstream region, perspective view of the three-dimensional pressure iso-surface of the detonation wave: (a) annular RDC model and (b) cylindrical RDC model.

Figure 6 presents the spatio-temporal averaged distributions of heat release rate and Mach number along the axial direction of the RDC, which characterize the combustion and flow acceleration processes. The annular RDC case was reproduced based on the configurations reported in Ref. [13]. The heat release rate shown in Fig. 6 was calculated using the following definition[24]:

$$\dot{q}(y) = -\iint_{A(y)} \sum_{i} \dot{\omega}_{i} \ \Delta_{f} H_{i}^{0} \ dA \tag{1}$$

The heat release rate distribution shown in Fig. 6 indicated that intense combustion occurred near the base of the combustor (y = 0-5 mm), with almost no reaction observed beyond y = 5 mm in both cases. The region of high heat release was therefore identified as the detonation combustion zone, with combustion effectively completed around y = 5 mm. This combustion completion height was consistent with the theoretically estimated filling height. Such consistency can be attributed to the extremely short chemical timescale of the H_2-O_2 reaction relative to the fluid residence time. The Mach number distribution in Fig. 6 further illustrated the flow acceleration within the RDC in both cases. The Mach number increased steadily from the base of the combustor, with a distinct inflection point observed around y = 5 mm, corresponding to the completion of combustion. Downstream of this point, the flow was further accelerated by the expansion of detonation products and reached a choked condition at the entrance of the divergent nozzle. Supersonic exhaust was achieved in both cases at the nozzle exit into the external mainstream. These results demonstrate that detonation-induced combustion, even under conditions where the main fuel was passively injected into the RDC, effectively drove the acceleration of the flow. Moreover, a choked condition was properly established within the RDC, upstream of its junction with the external mainstream, thereby preventing backflow.

HiSST-2025-338 Page |7

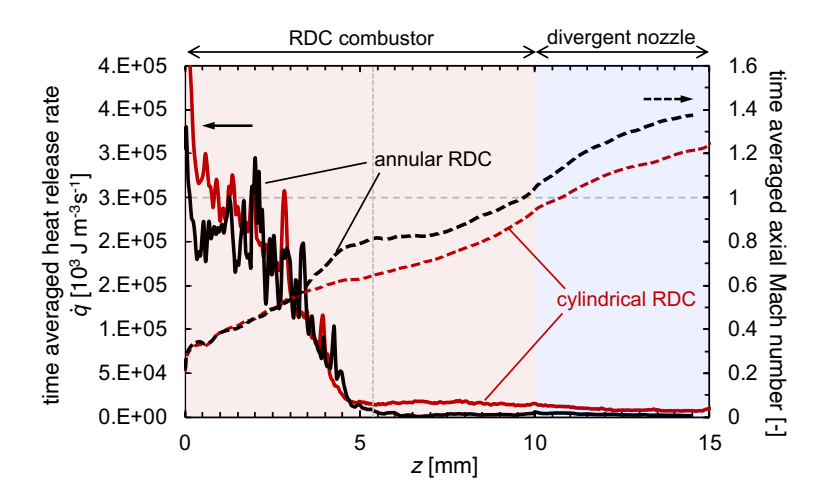


Fig 6. Axial distributions in the RDC section of heat release rate and Mach number for each case. The heat release rate is time-averaged, while all other quantities are averaged both temporally and spatially in the radial and azimuthal directions. The annular RDC case was reproduced based on the configurations reported in Ref. [13].

Figure 7 shows (a) the time evolution of the hydrogen distribution and (b) the time-averaged one-dimensional profile at the exit of the cylindrical RDC. In the figure, regions with hydrogen were indicated in red, while regions with burned gas were shown in light blue. The time-resolved visualization was obtained using the same time interval as that used in Fig. 5. For reference, the mole fraction distribution of hydrogen at the exit of the annular RDC was also included in Fig. 7(b). As shown in Fig. 7(a), the hydrogen distribution exhibited unsteady behavior over time. In particular, the hydrogen-rich region rotated slightly along the wall, following the rotational propagation of the detonation wave. Additionally, hydrogen was more concentrated near the center of the combustor compared to the near-wall region. Figure 7(b) presented the time-averaged mole fraction of hydrogen along the centerline of the cylindrical RDC exit. This profile indicated that hydrogen was distributed more broadly compared to the annular RDC case, suggesting that a significant amount of hydrogen remained mixed with the burned gas at the combustor exit and was subsequently discharged into the supersonic mainstream.

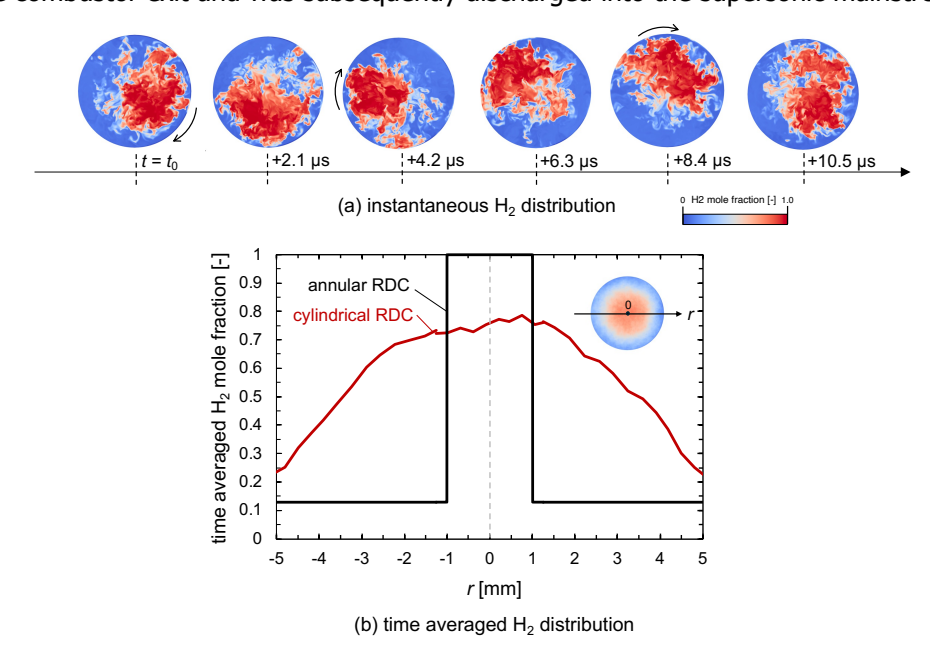


Fig 7. (a)instantaneous and (b) time averaged, H₂ distribution at the exit of the cylindrical RDC.

5.2. Mainstream Dynamics and Combustion Characteristics

Figure 8 shows instantaneous visualizations on the centerline (z-direction) cross-sectional plane for each case: (a) mole fraction of hydrogen, (b) mole fraction of OH radicals, and (c) temperature distribution. The baseline and annular RDC cases were reproduced based on the configurations reported in Ref. [13]. From the results in Fig. 8(a) and 8(b), it was observed that in all three models—the baseline model, the annular RDC model, and the cylindrical RDC model—the main fuel was injected into the supersonic flow and was gradually consumed downstream through interaction with the oxidizer in the mainstream. In particular, Fig. 8(a) shows that the hydrogen mole fraction decreased more rapidly in both RDC models than in the baseline model. The baseline case exhibited a highly steady hydrogen distribution, while both the annular and cylindrical RDC models showed greater unsteadiness due to enhanced jet penetration and stronger fuel-oxidizer interaction. However, the distributions in the annular and cylindrical RDC models were largely similar in terms of penetration height and the level of fluctuations. This indicates that the difference in combustor geometry between the annular and cylindrical configurations had minimal effect on the overall combustion behavior in this flow regime. Figures 8(b) and 8(c) further demonstrated that, compared to the baseline model, both RDC models exhibited higher OH* concentrations and higher temperatures near the lower wall, indicating more intense combustion in that region.

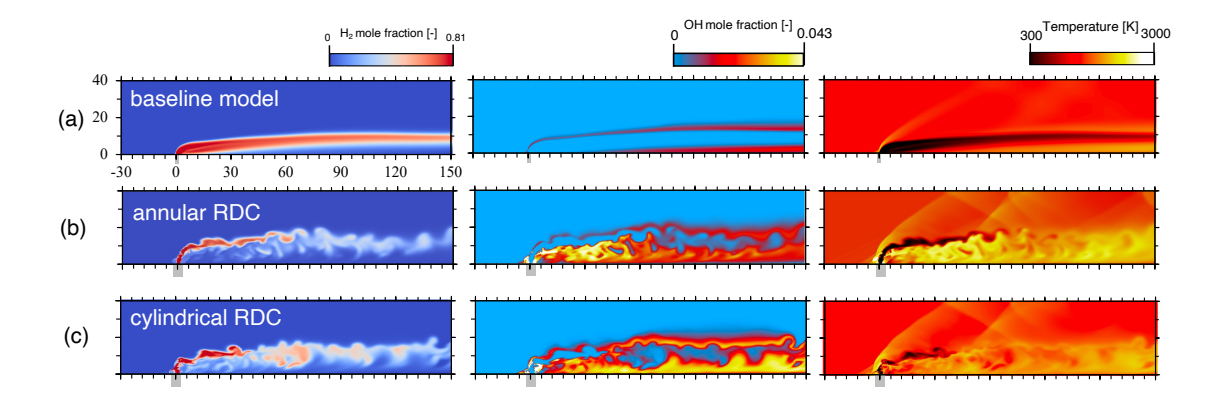


Fig. 8 Instantaneous fields at the center plane ($z = 22.5 d_{tuel}$): (a) baseline model, (b) annular RDC model, and (c) cylindrical RDC model. The baseline and annular RDC cases were reproduced based on the configurations reported in Ref. [13].

Figure 9 presents a quantitative comparison of the time-averaged fuel consumption rate for each model. Solid lines indicate the mean values computed along the streamwise direction. In the figure, blue, black, and red correspond to the baseline, annular RDC, and cylindrical RDC models, respectively. The baseline and annular RDC cases were reproduced based on the configurations reported in Ref. [13]. The fuel consumption rate was evaluated based on the mass flow rate of unburned fuel along the x-axis, using the following definition:

$$\eta_{\dot{m}}(x) = 1 - \frac{\dot{m}_{\text{H}_2}(x)}{\dot{m}_{\text{H}_2,\text{jet}}}$$
(2)

The cylindrical RDC model demonstrated a fuel consumption rate comparable to that of the annular RDC model, indicating that the geometric simplification did not compromise combustion performance. Moreover, compared to the baseline model, the cylindrical RDC achieved the same level of fuel consumption 23.3% earlier along the combustor axis. This result suggests that the use of a cylindrical RDC enables a more compact combustor design while maintaining high combustion efficiency. In other

HiSST-2025-338 Page |9 Numerical Investigation on the Optimization of a Detonation-Assisted Fuel Injection System

words, even without an inner cylinder, the configuration in which the main fuel is injected from inside the combustor was able to sustain a combustion performance comparable to that of the annular RDC model.

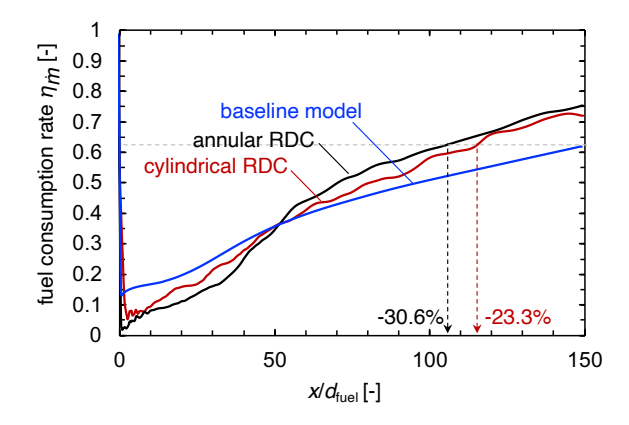


Fig 9. Streamwise distributions in the mainstream region of fuel consumption rate in the mainstream region. The blue line denotes the baseline model and the black line shows the annular RDC model reported in ref [13]. The red line represents the cylindrical RDC injection model.

6. Conclusion

To enhance the practicality of the previously proposed detonation-assisted fuel injection system employing an annular rotating detonation combustor (RDC), this study introduced a simplified configuration utilizing a cylindrical RDC. In both configurations, unsteady detonation products containing pressure disturbances and reactive radicals—were injected into a Mach 2.4 supersonic crossflow to assist and enhance combustion.

The analysis revealed that the cylindrical RDC sustained stable detonation propagation and intense combustion within a confined region near the combustor base. The main fuel, introduced directly from the bottom wall, was entrained by the rotating detonation front and exhibited a spiraling distribution as it was discharged toward the combustor exit. This behavior was accompanied by efficient mixing with the oxidizer and heat release, resulting in effective flow acceleration and the establishment of a choked condition at the nozzle entrance.

Notably, the fuel consumption rate of the cylindrical RDC was found to be comparable to that of the annular RDC, despite its simpler geometry. Compared to the baseline model, the cylindrical RDC achieved the same level of fuel consumption 23.3% earlier along the combustor axis, suggesting a significant potential for combustor length reduction. These findings demonstrate that even with a single-cylinder configuration and bottom-mounted fuel injection, high combustion efficiency can be maintained. The cylindrical RDC thus offers a more compact and structurally practical alternative to the annular RDC, while preserving the benefits of thermal and chemical assistance provided by detonation products. This configuration holds promise for future integration into realistic scramjet engine systems.

HiSST-2025-338 Page |10 Copyright © 2025 by author(s)

Acknowledgments

This study was financially supported by JSPS KAKENHI Grants No. JP23K20036, JP23H05446, JP25KJ2066, and by the Institute of Space and Astronautical Science of the Japan Aerospace Exploration Agency. In addition, this work is supported by "Joint Usage/Research Center for Interdisciplinary Large-scale Information Infrastructures (JHPCN)" and "High Performance Computing Infrastructure (HPCI)" in Japan (Project ID: jh230050, jh240048, jh250026, hp250122). Part of the numerical results in this research were obtained using supercomputing resources at Cyberscience Center, Tohoku University.

References

- 1. D. Musielak, Scramjet propulsion: a practical introduction, John Wiley & Sons, Incorporated, Hoboken, New Jersey (2023).
- 2. K. Tani, M. Takegoshi, K. Takasaki, S. Tokudome, JAXA RD1 Flight Experiment on Supersonic Combustion: Part 1. Overview, 25th AIAA International Space Planes And Hypersonic Systems And Technologies Conference (2023).
- 3. K.P. Katz, Road to Mach 10: Lessons Learned from the X-43A Flight Research Program, Air & Space Power Journal 25 (2011) 121.
- 4. T. Ledbetter, Test Flight Of X-51A Vehicle Partially Successful, Officials Investigate, Inside the Pentagon's Inside the Air Force 21 (2010).
- 5. M.K. Smart, N.E. Hass, A. Paull, Flight Data Analysis of the HyShot 2 Scramjet Flight Experiment, AIAA Journal 44 (2006) 2366–2375.
- 6. HIFIRE direct-connect rig (HDCR) Phase I scramjet test results from the nasa langley arc-heated scramjet test facility, 17th AIAA International Space Planes and Hypersonic Systems and Technologies Conference (2011).
- 7. G. Choubey, Scramjet combustion: fundamentals and advances, Butterworth-Heinemann, Oxford, England (2022).
- 8. A review of air-fuel mixing and alternative methods in scramjets and scramjet-like engines, J. Br. Interplanet Soc. 69 (2016) 116–126.
- G. Choubey, M. Solanki, O. Patel, Y. Devarajan, W. Huang, Effect of different strut design on the mixing performance of H2 fueled two-strut based scramjet combustor, Fuel. (Guildford) 351 (2023) 128972.
- 10. K. Venkateswarlu, S.V.K. Reddy, The Influence of Strut Injection Methods on Flame Stabilization and Combustion Performance of Scramjet Engines: A Review, International Journal of Aeronautical and Space Sciences (2025).
- 11. S. Roga, CFD Analysis of Scramjet Engine Combustion Chamber with Alternating Wedge-Shaped Strut Injector at Flight Mach 6.5, J. Phys. Conf. Ser. 1276 (2019) 12038.
- 12. S. Wang, Z. Du, W. Huang, G. Choubey, Numerical study on a novel device for hydrogen mixing enhancement in a scramjet engine: Coaxial injector, Aerosp. Sci. Technol. 127 (2022) 107680.
- 13. M. Miyashita, A. Matsuo, E. Shima, A. Kawasaki, N. Itouyama, K. Matsuoka, J. Kasahara, Numerical investigation of a detonation-assisted fuel injection system in supersonic crossflow, Combustion and Flame, Accepted for Publication (2025).
- 14. J. Shepherd, Detonation-Waves and Propulsion, Combustion in High-Speed Flows, Kluwer Academic Publ, Dordrecht (1994) 373–420.
- 15. W. Fickett, Detonation: Theory and Experiment, Dover Publications, Newburyport (2012).
- 16. M. Gamba, M.G. Mungal, Ignition, flame structure and near-wall burning in transverse hydrogen

- jets in supersonic crossflow, J. Fluid Mech. 780 (2015) 226-273.
- 17. Y. Wada, M.S. Liou, An accurate and robust flux splitting scheme for shock and contact discontinuities, SIAM Journal of Scientific Computing 18 (1997) 633-657.
- 18. S. Yamamoto, H. Daiguji, Higher-order-accurate upwind schemes for solving the compressible Euler and Navier-Stokes equations, Comput. Fluids 22 (1993) 259-270.
- 19. S. Gottlieb, C.-W. Shu, Total variation diminishing Runge-Kutta schemes, Math. Comput. 67 (1998) 73-85.
- 20. Z. Hong, D.F. Davidson, R.K. Hanson, An improved H2/O2 mechanism based on recent shock tube/laser absorption measurements, Combust. Flame 158 (2011) 633-644.
- 21. Coefficients for calculating thermodynamic and transport properties of individual species, National Aeronautics and Space Administration, Office of Management, Scientific and Technical Information Program, Washington, DC (1993).
- 22. Sanford., Computer program for calculation of complex chemical equilibrium compositions and applications supplement I--Transport properties, National Aeronautics and Space Administration, Lewis Research Center.
- 23. D.C. Wilcox, Turbulence modeling for CFD, 3rd ed., DCW Industries, La Canada, Calif (2006).
- 24. T. Poinsot, D. Veynante, Theoretical and numerical combustion. 2nd ed., Edwards, Philadelphia (2005).

HiSST-2025-338 Page |12